

Parametric excitations of trapped ions in a linear rf ion trap

X. Zhao, V. L. Ryjkov, and H. A. Schuessler

Department of Physics, Texas A & M University, College Station, Texas 77843

(Received 1 August 2002; published 26 December 2002)

The parametric resonant behavior of ions inside a linear rf ion trap is studied both theoretically and experimentally. Theoretically, the resonant motion of ions inside an ideal ion trap is described by approximating the trapping rf field as a harmonic pseudopotential with the ions being excited by an additional quadrupolar ac voltage. The resulting damped Mathieu equation is studied and the regions of resonant instability are predicted by investigating the solutions. Experimentally, the parametric excitation of Mg^+ ions is observed by subjecting the cloud of trapped ions to an additional quadrupolar ac field. The various ion motion resonances are detected through the disappearance of the laser-induced fluorescence signal. Weak damping is introduced by the presence of a low-pressure buffer gas. The experimental results are compared with the theoretical predictions.

DOI: 10.1103/PhysRevA.66.063414

PACS number(s): 32.80.Pj, 07.75.+h

I. INTRODUCTION

rf ion traps have been used for a wide range of applications, such as mass spectrometry, laser spectrometry [1,2], frequency standards [3], ion-molecule collisions [4], laser cooling and ion crystallization [5–9], to name a few. The detailed knowledge of the trapped ion motion is crucial for many and important to all of the applications. For ion manipulation and detection, dipole excitation [10] is the usual choice. However, recently several research groups have also demonstrated excitation of the trapped ion resonant motion under the influence of an auxiliary ac quadrupolar field applied in addition to the rf trapping potential [11–17]. This kind of resonance of the trapped ions is an example of parametric resonance [18,19].

So far, most of the research effort in this area has been concentrated on the traditional three-dimensional (3D) Paul trap configuration. Using perturbation theory, Sudakov *et al.* [11] derived that the quadrupole excitation angular frequencies ω_r^n can be described by

$$\omega_r^n = \frac{\Omega}{n} |r + \beta|, r = 0, \pm 1, \pm 2, \dots, \quad (1)$$

where Ω is the frequency of the rf trapping potential; $n = 1, 2, \dots$ is the order of the parametric excitation; β is a dimensionless fractional number that is determined by the operating parameters of the trap; r and β determine the frequencies of ion micromotion oscillations in the absence of the parametric excitation voltage. Experimentally, Vedel and Vedel [12] observed the quadrupolar excitation of the ions for $r=0$, $n=1$ and 2. Resonances of the ion cloud for up to $n=10$ were observed by Razvi *et al.* [13]. The same group of researchers identified the nonlinear collective oscillations of an ion cloud in a Paul trap, and gave a detailed numerical analysis to support their conclusions [14]. Later on, Chu *et al.* [15] reported their observations of higher-order resonances for up to $r=4$ and the high-order-combined oscillations. Although there are many things in common for the ion motions in a 3D Paul trap and a linear rf ion trap, there are also distinctive differences. Kononkov *et al.* discussed and verified the prediction of the modified stability diagram due

to the quadrupolar rf excitation field in their work [16] for a quadrupole mass filter. They also compared their experimental results with the theoretical mapping of the stability diagram. Collings and Douglas [17] measured the resonances of the trapped ions for $r=0$, $n=1$ to $n=6$, through fragmentation of protonated reserpine in a linear rf ion trap.

In this paper we present our work on the parametric resonances of the trapped ions in a linear rf ion trap. We obtain an analytical description of the parametric resonance in the ion trap by approximating the rf trapping potential with the pseudopotential model, in which the ions inside the trap see a harmonic potential well. When the auxiliary ac voltage is applied, the ions are subject to an additional force. We also incorporate damping into the equations of motion and show that the parametric excitation is described by the canonical Mathieu equation. The Mathieu equation, commonly used in the ion trapping theory to describe *trapping* of the ions, is applied here to describe the *parametric excitation* of the trapped ions. As a result, the parameters of the ac quadrupole excitation field determine the position of the operating point on the stability diagram of the secular motion. We found that for parametric resonance to occur the excitation frequency must belong to one of the frequency intervals. The boundaries of these frequency intervals vary with the amplitude of the excitation. The boundaries of orders 1 and 2 were measured and compared with the ideal theoretical predictions made in this paper.

The detection method used in our experiments is optical. The ion cloud inside the trap is overlapped with a frequency doubled laser beam, and the ion motions under the parametric excitations are detected by observing the change of the laser-induced fluorescence (LIF).

II. ION TRAP

Figure 1 shows the linear rf trap used for these measurements. The trap consists of four identical cylindrical rods, 6 mm in diameter. Each rod is divided into three equal 5-cm-long segments for dc manipulation. All segments of the same rod have the same rf voltage. The quadrupole rf trapping potential is created by applying rf voltage to the rods symmetrically as shown in the figure. The distance from the axis

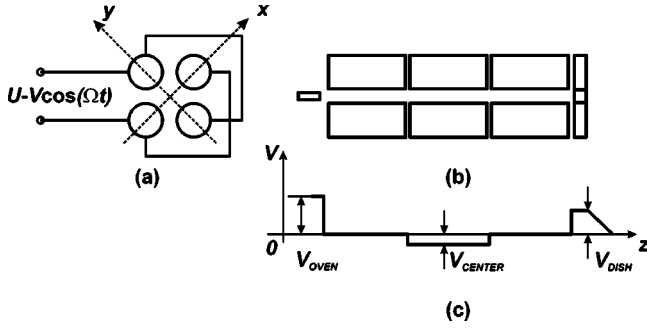


FIG. 1. Schematic representation of the trap. (a) Cross-section view of the ion trap. Each opposing pairs of the trap electrodes are wired together for the same rf voltage. The (x, y) plane is chosen so that each axis goes from the center of the trap area to one electrode. (b) Longitudinal view of the trap. The two end electrodes (the cylinder on the left and the dish on the right) are also shown. (c) A typical dc voltage distribution along the z axis to provide longitudinal ion confinement.

of the ion trap to the surface of each rod is $r_0 = 2.61$ mm, chosen to minimize the anharmonicity of the trapping potential [20].

First let us consider the trapping in the direction perpendicular to the trap electrodes. We choose the coordinates as shown in Fig. 1, placing the z axis along the longitudinal direction of the trap. The time dependent rf potential around the center of the trap is then

$$\phi(x, y; t) = [U - V^{(p-p)} \cos(\Omega t)] \frac{x^2 - y^2}{2r_0^2}, \quad (2)$$

where $-V^{(p-p)} \cos(\Omega t)$ is the applied rf signal, the operating rf frequency is $\Omega/2\pi = 7.37$ MHz, U is the quadrupole dc offset, usually 0 in all our measurements. This rf potential provides the radial confinement of the ions.

The equations of motion of a particle of mass m and charge e can be described by the canonical Mathieu differential equation,

$$\frac{d^2 u}{d\eta^2} + [a - 2q \cos(2\eta)] u = 0, \quad (3)$$

with $u = x$ or y , and

$$a = a_x = -a_y = \frac{4eU}{mr_0^2 \Omega^2}, \quad (4a)$$

$$q = q_x = -q_y = \frac{2eV^{(p-p)}}{mr_0^2 \Omega^2}, \quad (4b)$$

$$\eta = \frac{\Omega t}{2}. \quad (4c)$$

Therefore, the ion motion in x and y directions is described by the solutions of the Mathieu equation, which is well studied [21,22]. The solutions of the Mathieu equation exhibit

both stable and unstable behaviors. The stability of the solution is determined by the values of the parameters a and q . The stability of the ion motion is best illustrated by the well-known [23,24] stability (a, q) diagram. The stable regions in the (a, q) plane are utilized for ion trapping. The (a, q) parameters used for trapping the ions in the measurements presented in this paper fall into the lowest stable region.

Along the z direction, the ions are confined by the applied dc voltages, as shown in Fig. 1(c). In the central region of the trap, the dc potential is constant, therefore, the ion motion along the z axis is approximated by that of a free ion.

The pseudopotential model [25] is a useful simplification designed to describe the secular motion of the trapped ions. It can be described as the effective potential of the time averaged ponderomotive force of an rf field. The pseudopotential, denoted by $\Psi(x, y)$, can be written in terms of the spatial part of the time dependent rf potential $\phi(x, y)$ as

$$\Psi(x, y) = \frac{e}{4m\Omega^2} \left[\left(\frac{\partial \phi}{\partial x} \right)^2 + \left(\frac{\partial \phi}{\partial y} \right)^2 \right]. \quad (5)$$

When combining this formula and Eq. (2), the pseudopotential of the *trapping* quadrupole rf field takes the form

$$\Psi(x, y) = \frac{\bar{D}}{r_0^2} (x^2 + y^2), \quad (6)$$

where \bar{D} , the potential depth, is defined by

$$\bar{D} = \frac{eV_0^2}{m\Omega^2 r_0^2}, \quad (7)$$

with V_0 being the amplitude of the rf voltage. The potential depth of the trap is the potential difference between the trap center and trap electrodes.

With the pseudopotential model, a trapped ion sees an effective simple harmonic potential. The Hamiltonian of the trapped ion in the radial direction is, therefore, that of a simple harmonic oscillator. The secular frequency is

$$\omega_s = \frac{\sqrt{2}eV_0}{m\Omega r_0^2} = \frac{eV^{(p-p)}}{\sqrt{2}m\Omega r_0^2}. \quad (8)$$

III. PARAMETRIC RESONANCE WITH DAMPING

In order to study the parametric resonance of the trapped ions, the trapping parameters, the rf and dc voltages and, as a result the secular frequency ω_s and the trapping characteristic values (a, q) , are kept the same throughout the measurements. Then an additional *auxiliary* ac excitation voltage is applied to the trap electrodes. This excitation voltage produces a quadrupolar ac electric field in the trapping region because it is applied to the trap rods in the same way as the rf trapping voltages [see Fig. 1(a)]. This parametric excitation potential is given by the following expression:

$$V_p = \frac{-V_p^{(p-p)} \cos(\omega t)}{2r_0^2} (x^2 - y^2), \quad (9)$$

where $-V_p^{(p-p)} \cos(\omega t)$ is the applied driving voltage.

The equation of motion for a trapped ion in the harmonic pseudopotential (6) under the influence of the quadrupolar excitation (9) and in the presence of a dissipative force is

$$\frac{d^2x}{dt^2} + 2\kappa\omega_s \frac{dx}{dt} + \omega_s^2 [1 - 2\epsilon \cos(\omega t)]x = 0, \quad (10)$$

where the term $2\kappa\omega_s$ describes the damping which is proportional to the speed of the ion. Substitutions of $x(t) = e^{-\kappa\omega_s t} u(t)$ and $\omega t/2 = \eta$ transform this equation into the canonical form of the Mathieu equation,

$$\frac{d^2u}{d\eta^2} + [a' - 2q' \cos(2\eta)]u = 0, \quad (11)$$

with the following parameters:

$$a' = \left(\frac{2\omega_s}{\omega}\right)^2 (1 - \kappa^2), \quad (12a)$$

$$q' = \frac{\epsilon}{1 - \kappa^2} a' = \epsilon \left(\frac{2\omega_s}{\omega}\right)^2, \quad (12b)$$

$$\epsilon = \frac{eV_p^{(p-p)}}{2mr_0^2\omega_s^2}. \quad (12c)$$

One notices that the characteristic value a' is dependent on the damping factor κ , while q' is not; and q' is proportional to the strength of external excitation.

Clearly, the motion of a trapped ion is again described by the Mathieu equation, even though the trapped ions are subject to the influence of an additional ac voltage, the parametric excitation voltage V_p . The secular motion of the trapped ions exhibits stable or unstable behavior depending on the values of the characteristic parameters a' and q' . For a given trapping potential, i.e., a given secular frequency, these characteristic values are only determined by the applied parametric excitation voltage. When the characteristic values fall into the unstable regions on the (a', q') plane, parametric resonance occurs. Therefore, the unstable regions in the (a', q') plane are the parametric resonance regions. For our measurements it was found that the damping factor κ is very small, and consequently parametric resonance of the trapped ions occurs in the vicinity of $2\omega_s/\omega = n^2$, $n = 1, 2, 3, \dots$, same as in the case of no damping. In the following, the number n is called the order of parametric resonance.

Combining the variable substitution of $x(t) = e^{-\kappa\omega_s t} u(t)$ with the general form of the unstable solutions of Mathieu equation, for an operating point of (a', q') lying in the unstable area, the solution for the original equation of motion can be written as

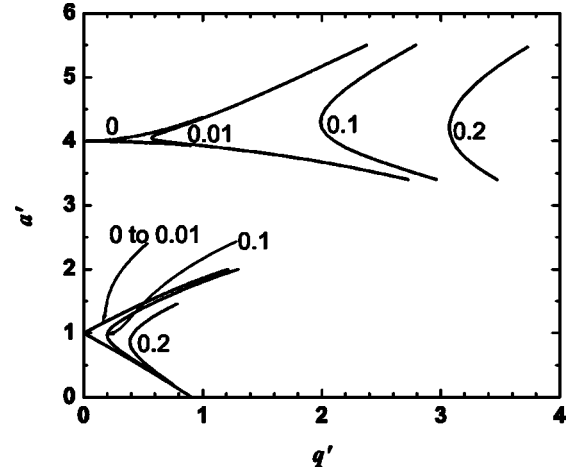


FIG. 2. The unstable regions for various values of μ .

$$x(t) = A e^{[\mu - \kappa(2\omega_s/\omega)](\omega t/2)} \sum_{r=-\infty}^{\infty} c_r e^{ir(\omega t/2)} + B e^{-[\mu + \kappa(2\omega_s/\omega)](\omega t/2)} \sum_{r=-\infty}^{\infty} c_r e^{-ir(\omega t/2)}, \quad (13)$$

where A, B are constants determined by the initial conditions; μ is the characteristic exponent of the solution of the undamped Mathieu equation with parameters q' and a' , and is real and positive; r can be even or odd depending on where the values of (a', q') lie on the (a', q') plane.

The second term in Eq. (13) is always stable for positive real μ, κ . Instability arises from the first term when $\mu > \kappa(2\omega_s/\omega)$. Figure 2 displays the (a', q') diagram for various values of μ . The contours corresponding to a fixed value of μ are at the same time the boundaries that encircle the unstable region when the damping constant is $\kappa = \mu(\omega/2\omega_s)$.

The vertices of the unstable regions touch the a' axis in the case of undamped parametric excitation, indicating that an arbitrarily small excitation amplitude can produce exponentially increasing oscillations. In the case of damped parametric excitation the regions of instability move away from the a' axis. Since the value of q' is proportional to the applied excitation voltage, the excitation voltage necessary to parametrically excite the trapped ions increases as the damping is increased. The lowest possible excitation strength ϵ for a given order of parametric resonance n and fixed damping κ is called the *critical strength* $\epsilon_n^{(crit)}$. The critical strength increases as the order of the parametric resonance increases. For a given excitation strength, only the lower orders of the parametric resonance can occur; the higher the excitation strength, the more orders of resonance will be produced.

Figure 2 also illustrates that the frequency ranges in which the resonances occur are narrower for larger n . The width of the frequency range can be evaluated by the width of the boundary plots, which asymptotically approach the boundaries with the a' value being a'_n and b'_n .

TABLE I. Coefficients of the approximation $\epsilon_n^{(\text{crit})} = C_n \kappa^{1/n}$.

n	From Eq. (16)	From Ref. [13]
1	2	2.0
2	$\sqrt{2} \approx 1.414$	2.03
3	$\sqrt[4]{9} \sqrt[3]{18} \approx 1.165$	1.83
4	$\sqrt[2]{\frac{1}{2}} \sqrt[4]{18} \approx 1.030$	1.73
5	$\sqrt[8]{\frac{8}{25}} \sqrt[5]{225} \approx 0.945$	1.73
6	$\sqrt[2]{\frac{6}{9}} \sqrt[6]{4050} \approx 0.887$	

In all our measurements, the applied excitation frequencies satisfy $|\omega/2 - \omega_s| \ll \omega_s$, therefore, $\mu - \kappa(2\omega_s/\omega) \approx \mu - n\kappa$ is a very good approximation. With this approximation and the properties of iso- μ plots of the Mathieu equation [21], the damping factor in the neighborhood of the n th order of parametric resonance can be written as

$$\mu^2 = (n\kappa)^2 = \frac{(a'_n - a')(a' - b'_n)}{4n^2}. \quad (14)$$

μ reaches a maximum when a' is the midpoint $a' = (a'_n + b'_n)/2$. This point is the vertex of the unstable region in the (a', q') plane. Thus, for a given value of q' , the maximum possible damping constant κ for which the resonance will still occur is given by

$$\kappa = \frac{\mu}{n} = \frac{a'_n - b'_n}{4n^2}. \quad (15)$$

Equation (15) will be used later to estimate the damping factors. The series expansions of a'_n and b'_n for small q' are known [26], and can be used to obtain the simplified expression for the critical excitation strength. Since, for small κ , $q' \approx \epsilon^{(\text{crit})} n^2$, and $a'_n - b'_n = A_n q'^n + o(q'^n)$ we obtain the expression for the critical strength of the n th order parametric excitation,

$$\epsilon_n^{(\text{crit})} \approx \left(\frac{4n^2}{A_n} \right)^{1/n} \frac{\kappa^{1/n}}{n^2} = C_n \kappa^{1/n}. \quad (16)$$

The resulting coefficients C_n are compiled in Table I. The values listed in the second column of Table I are the result of a computer simulation [13].

The difference of the two roots of the quadratic equation (14) gives the width $\Delta a'$ of the unstable region across the a' axis for a fixed value of excitation strength,

$$\begin{aligned} \Delta a' &= (a'_n - b'_n) \sqrt{1 - \frac{16n^4 \kappa^2}{(a'_n - b'_n)^2}} \\ &= \Delta a' |_{\kappa=0} \sqrt{1 - \frac{16n^4 \kappa^2}{(\Delta a' |_{\kappa=0})^2}}. \end{aligned} \quad (17)$$

Apparently, the width decreases as the damping increases.

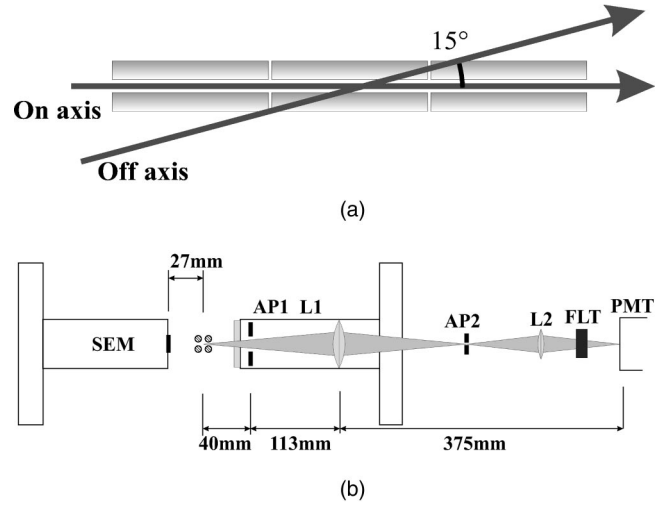


FIG. 3. Schematic diagram of the optical detection setup. (a) Different orientations of the UV beam. (b) Detection arrangement.

IV. EXPERIMENTAL METHODOLOGY

The parametric resonance features of the trapped ions were investigated by detecting the change of the LIF signal of the trapped Mg^+ ions.

The Mg^+ ions are generated by electron bombardment of the neutral thermal Mg atoms. This is realized by a pair of atom oven and electron gun mounted perpendicularly to each other and to the trap electrodes. The atom oven and the electron gun are located outside one group of the outer segments of the trap electrodes. Upon generation, the Mg^+ ions are first cooled by the presence of helium buffer gas at a pressure of about 10^{-6} Torr. Then due to the lower dc voltages applied on the central trap segments along the z axis, these trapped ions move to the central region of the ion trap. In the central region, the trapped ions are overlapped by a UV beam at a wavelength of 280 nm. As shown in Fig. 3(a), there are two ways to overlap the UV beam with the ion cloud, one is on axis, the other is off axis. For the results presented, the on-axis configuration is used. The UV beam is obtained by frequency doubling a cw ring dye laser (Coherent 699) in an external buildup cavity [27].

Figure 3(b) illustrates how the ions and their optical signals are detected. The secondary electron multiplier (SEM) is mounted inside the vacuum chamber close to and perpendicular to the trap electrodes on one side of the trap. On the opposite side, the flange with a quartz window, through which the optical signals are collected on to the photomultiplier tube (PMT), is mounted in the same manner as the SEM. They are centered to the central segments of the trap electrodes. The SEM is used throughout this work for ion counting upon their ejection from the trap; and the PMT is used to detect the LIF signal of the trapped ions.

Parametric resonance of the trapped ions can be observed by monitoring the change of the LIF signal. When the applied parametric excitation frequency is swept, while its amplitude is kept constant, at some point the ions of proper mass m and charge e will undergo parametric resonance with the applied signal. As a result, the ions are heated and their

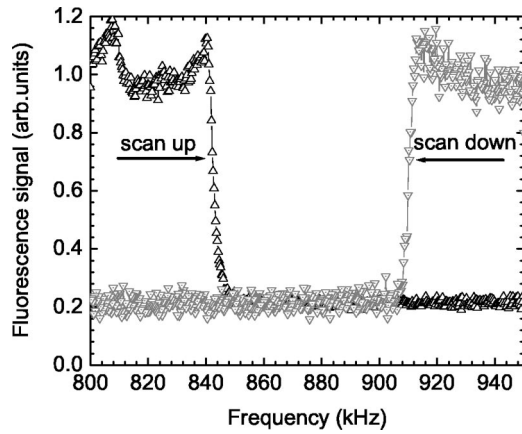


FIG. 4. LIF signal obtained from parametric excitation of the Mg^+ ions. The order of parametric excitation is $n=1$. The peak-to-peak value of the trapping potential is $V^{(p-p)}=287$ V.

Doppler linewidth is increased. For a small enough excitation strength, the ions will not be lost from the trap. In that case, when the parametric resonance condition is removed, the ions will quickly regain the temperature they had before the excitation through collisions with the buffer gas. The condition for parametric resonance in this paper was that the ions were ejected from the trap. In this case the LIF signal drops to the background level. The UV radiation power was only a few μW and was detuned far from resonance. This was done to avoid strong laser cooling [27] and to investigate the buffer gas cooling effects unobstructed. To check this condition, the frequency of the UV light was scanned across the transition to verify that the LIF signal visually appears symmetric across the transition since laser cooling introduces asymmetry. To further minimize the cooling effects, the laser frequency was purposely detuned away from resonance by more than 2 GHz during the measurements.

For each parametric excitation order n , there is a range of frequencies under which the trapped ions can be parametrically excited. Measurements are made to find this range for each n . The experimental procedure is as follows. For a given trapping potential, the secular frequency ω_s is estimated. Then the relation $\omega=2\omega_s/n$ is used to find the frequency around which parametric resonance will occur for a particular n . Then the parametric excitation frequencies are swept from lower to higher values. The frequency, at which the LIF signal decreases sharply, indicates the lower boundary of the parametric resonance. To obtain the frequency of the upper boundary, the parametric excitation frequencies are scanned in the opposite direction, i.e., from higher to lower values. It should be noted that since for these measurements the parametric drive was strong enough to eject the ions from the trap, the ion trap had to be reloaded between subsequent scans. The number of ions in the trap throughout the measurements was around 10^4 .

Figure 4 is an example obtained from two of such opposite scans. It shows that for any applied parametric excitation frequency within the range of $842 \leq \omega/2\pi \leq 911$ kHz, the trapped ions will be under resonance.

With this procedure repeated for various applied excitation amplitudes, the boundaries of the regions, where para-

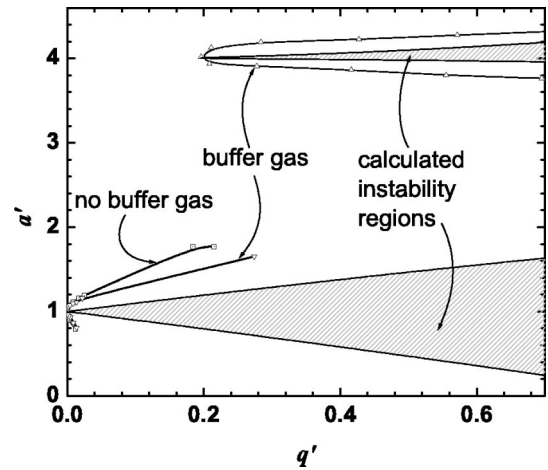


FIG. 5. The calculated and measured boundaries for $n=1$ and $n=2$.

metric resonance occurs, can be mapped out and the measured values are drawn on the (a', q') plane for each resonance order n .

V. RESULTS AND DISCUSSION

Using the method described in the preceding section, the lower and upper boundaries of the unstable regions were obtained. Figure 5 shows the results of such measurements together with the calculated results. The shaded areas are the calculated unstable regions for $n=1$ and $n=2$. The measured boundaries are obtained for different buffer pressures. The no buffer gas condition refers to the situation when there is no helium gas in the chamber, with the background pressure below 10^{-9} mbar. The other boundaries are obtained with a helium buffer gas pressure around 1.1×10^{-6} mbar.

A number of conclusions can be drawn from the results. From the two measured boundaries for different buffer gas pressures for the resonance order $n=1$, it is verified that the stronger the damping, the narrower the unstable region, i.e., the frequency range in which the parametric excitation can occur.

There are large deviations between the measured and calculated boundaries, since the measured boundaries are wider than their theoretical predictions for each order n . However, this can be explained as follows. Since we have classified the stable solutions as those which have a finite amplitude no matter how large it is, this ideal case does not match the experimental situation exactly. In a real experiment, as soon as the amplitude of the ion motion is larger than the size of the trapping region, the ions will be lost. This regime is then unstable in a finite-size trap while being classified as stable from the Mathieu equation standpoint. Therefore, this geometrical effect accounts for the cushion around the theoretically calculated stability boundary.

It was not possible for us to map out the boundaries of parametric excitation on the (a', q') plane for orders higher than $n=2$. This was caused by the the frequency response of our present trap circuit, which was designed to isolate unwanted sources of the parametric excitation voltage and the

TABLE II. Critical parametric excitation voltages. These are the minimum excitation voltage amplitudes needed to start any parametric resonance for different excitation orders (n).

n	Frequency (kHz)	V_c (mV)
1	860.75	16.5
2	436.5	625.8
3	291	1333

rf trapping potential. For the same reason, the lower branch of the boundary for $n=1$ was not mapped out further.

In addition to the frequency scans as described in the preceding section, we have also obtained the values of the critical excitation voltage V_c necessary to observe the parametric resonance. Such measurements were done by keeping the excitation frequency constant in the middle of the narrowest obtained interval of parametric resonance frequencies. Then the amplitude of the excitation was gradually increased until the LIF signal dropped indicating the onset of the parametric resonance. These critical excitation voltages are listed for several orders n in Table II. As expected, the critical excitation voltage increases with the order of resonance.

The effective damping factor κ can also be evaluated from the data in Table II. This evaluation was carried out for different buffer gas pressures and parametric excitation orders (n) using Eq. (15). The results are summarized in Table III. The values of the damping parameter κ are not very different for the three orders of parametric resonance that we observed. The damping factor increases by a factor of 30–40 when we introduce buffer gas.

Razvi *et al.* reported different behaviors of the odd and even resonances in their measurements of parametric resonance in the symmetrical rf Paul trap [13]. They found that the critical voltages for odd and even orders of the parametric resonance behave in a way that suggests that the values of the damping factor differ by three orders of magnitude, with the even orders having the smaller value. We were not able to observe this difference. While for our linear rf trap the values of κ for orders $n=1,3$ are closer to each other than to κ for $n=2$, the difference is not nearly as drastic as observed in Ref. [13]. Also, the even order has a larger value of κ .

It is also of interest to discuss the values of the oscillation

TABLE III. Damping parameters κ for the measured boundaries.

n	Pressure (mbar)	κ
1	$< 10^{-9}$	2.33×10^{-5}
1	1.1×10^{-6}	6.45×10^{-4}
2	1.3×10^{-6}	1.20×10^{-3}
3	1.3×10^{-6}	7.09×10^{-4}

decay rates $\Gamma = 2\kappa\omega_s$ for the two trap geometries. In our linear trap we observe decay rate $\Gamma_{\text{vac}} \approx 20 \text{ s}^{-1}$ under high vacuum conditions. Comparing this number to the corresponding high vacuum values of $\Gamma_{\text{even}} = 0.25 \text{ s}^{-1}$ and $\Gamma_{\text{odd}} = 580 \text{ s}^{-1}$ reported in Ref. [13] for the symmetrical trap, we notice that our value falls in between those values. When the buffer gas was present we observed an increased decay rate of $\Gamma_{\text{buff}} \approx 600 \text{ s}^{-1}$. These differences can be attributed to the different trap geometries as well as differences in theoretical treatment of the experimental results.

VI. CONCLUSIONS

We have demonstrated that the damped parametric excitation of the trapped ions inside a linear ion trap can be described by a set of Mathieu equations. Parametric resonance of the trapped ions occurs over a range of frequencies for each resonance order. For each order this frequency range varies with the amplitude of the excitation. The regions of instability on the (a', q') plane correspond to the parametric resonance. We experimentally mapped the actual boundaries for the regions where the parametric resonance occurs in an rf linear ion trap. We found that the Mathieu equation description of the parametric resonance reproduces the observed behavior quite well. However, the theoretically predicted unstable regions are somewhat narrower than the experimental ones. We attribute this observation to the finite size of the ion trap, since the theoretical treatment outlined in this work does not contain information about the amplitude of the induced oscillations.

ACKNOWLEDGMENT

This work was supported by the Welch foundation, Grant No. A-1546.

-
- [1] G.Z.K. Horvath, R.C. Thompson, and P.L. Knight, *Contemp. Phys.* **38**, 25 (1997).
 - [2] F.A. Londry and R.E. March, *Int. J. Mass Spectrom. Ion Processes* **144**, 87 (1995).
 - [3] D.J. Berkeland, J.D. Miller, J.C. Berquist, W.M. Itano, and D.J. Wineland, *Phys. Rev. Lett.* **80**, 2089 (1998).
 - [4] M. Welling, H.A. Schuessler, R.I. Thompson, and H. Walther, *Int. J. Mass Spectrom. Ion Processes* **172**, 95 (1998).
 - [5] D.J. Wineland and W.M. Itano, *Phys. Today* **40**, 34 (1987).
 - [6] F. Diedrich, E. Peik, J.M. Chen, W. Quint, and H. Walther, *Phys. Rev. Lett.* **59**, 2931 (1987).
 - [7] M. Drewsen, C. Brodersen, L. Hornekaer, and J.S. Hangst, *Phys. Rev. Lett.* **81**, 2878 (1998).
 - [8] W. Alt, M. Block, P. Seibert, and G. Werth, *Phys. Rev. A* **58**, R23 (1998).
 - [9] R. Blumel, C. Kappler, W. Quint, and H. Walther, *Phys. Rev. A* **40**, 808 (1989).
 - [10] H.A. Schuessler, E.N. Fortson, and H.G. Dehmelt, *Phys. Rev.* **187**, 5 (1969).
 - [11] M. Sudakov, N. Konenkov, D.J. Douglas, and T. Glebova, *J. Am. Soc. Mass Spectrom.* **11**, 10 (2000).
 - [12] F. Vedel and M. Vedel, *Int. J. Mass Spectrom. Ion Processes*

- 99**, 125 (1990).
- [13] M.A.N. Razvi, X.Z. Chu, R. Alheit, G. Werth, and R. Blumel, *Phys. Rev. A* **58**, R34 (1998).
- [14] R. Alheit, X.Z. Chu, M. Hofer, M. Holzki, and G. Werth, *Phys. Rev. A* **56**, 4023 (1997).
- [15] X. Chu, M. Holzki, R. Alheit, and G. Werth, *Int. J. Mass Spectrom. Ion Processes* **173**, 107 (1998).
- [16] N.V. Kononov, L.M. Cousins, V.I. Baranov, and M.Y. Suda-kov, *Int. J. Mass Spectrom. Ion Processes* **208**, 17 (2001).
- [17] B.A. Collings and D.J. Douglas, *J. Am. Soc. Mass Spectrom.* **11**, 1016 (2000).
- [18] L.D. Landau and E.M. Lifshitz, *Mechanics* (Pergamon Press, Oxford, England, 1960).
- [19] *Basic Theory of Oscillations*, edited by V.V. Migulin (Mir, Moscow, 1983).
- [20] C.-S. O and H.A. Schuessler, *Int. J. Mass Spectrom. Ion Phys.* **35**, 305 (1980).
- [21] N.W. McLachlan, *Theory and Application of Mathieu Functions* (Dover Publication, New York, 1964).
- [22] F.M. Arscott, *Periodic Differential Equations; An Introduction to Mathieu, Lamé and Allied Functions* (Macmillan, New York, 1964).
- [23] P.H. Dawson, *Quadrupole Storage Mass Spectrometry & Its Applications* (Elsevier, Amsterdam, 1976), Chaps. I, II, III, IV, V.
- [24] R.E. March and R.J. Hughes, *Quadrupole Storage Mass Spectrometry* (Wiley, New York, 1989).
- [25] H.G. Dehmelt, *Adv. At. Mol. Phys.* **3**, 53 (1967).
- [26] *Handbook of Mathematical Functions*, 10th ed., edited by M. Abramowitz and I.A. Stegun (NBS, Washington, 1972).
- [27] X. Zhao, Ph.D. thesis, Texas A&M University, 2001 (unpublished).